

Geophysical Research Letters®










RESEARCH LETTER

10.1029/2023GL103257

Focused Mid-Crustal Magma Intrusion During Continental Break-Up in Ethiopia

Key Points:

- We determine magma storage conditions in the Main Ethiopian Rift through geochemical analysis of olivine-hosted melt inclusions
- Volatile saturation barometry reveals that basaltic melts are focused at 10–15 km depth in the Ethiopian crust
- Geochemical heterogeneity in melt inclusions suggests that magma storage is likely to occur in semi-discrete sills

Kevin Wong^{1,2} , David Ferguson¹ , Penny Wieser³ , Daniel Morgan¹, Marie Edmonds⁴ , Amdemichael Zafu Tadesse^{5,6} , Gezahegn Yirgu⁶, Jason Harvey¹ , and Samantha Hammond⁷ 

¹School of Earth and Environment, University of Leeds, Leeds, UK, ²Now at Dipartimento di Scienze Biologiche, Geologiche e Ambientali (BiGeA), Alma Mater Studiorum Università di Bologna, Bologna, Italy, ³Department of Earth and Planetary Science, University of California, Berkeley, Berkeley, CA, USA, ⁴Centre for the Observation and Modelling of Earthquakes, Volcanoes and Tectonics (COMET), Department of Earth Sciences, University of Cambridge, Cambridge, UK, ⁵Department of Geosciences, Environment and Society, Université Libre de Bruxelles (ULB), Bruxelles, Belgium, ⁶School of Earth Sciences, Addis Ababa University, Addis Ababa, Ethiopia, ⁷School of Environment, Earth and Ecosystems Sciences, The Open University, Milton Keynes, UK

Supporting Information:

Supporting Information may be found in the online version of this article.

Correspondence to:

K. Wong,
kevin.wong@unibo.it

Citation:

Wong, K., Ferguson, D., Wieser, P., Morgan, D., Edmonds, M., Tadesse, A. Z., et al. (2023). Focused mid-crustal magma intrusion during continental break-up in Ethiopia. *Geophysical Research Letters*, 50, e2023GL103257. <https://doi.org/10.1029/2023GL103257>

Received 11 FEB 2023
Accepted 30 MAY 2023

Author Contributions:

Conceptualization: Kevin Wong, David Ferguson, Daniel Morgan, Marie Edmonds, Gezahegn Yirgu
Formal analysis: Kevin Wong, David Ferguson, Penny Wieser, Marie Edmonds
Funding acquisition: Kevin Wong, David Ferguson, Daniel Morgan, Marie Edmonds, Gezahegn Yirgu
Investigation: Kevin Wong, David Ferguson, Penny Wieser, Jason Harvey, Samantha Hammond
Resources: Kevin Wong, David Ferguson, Amdemichael Zafu Tadesse, Gezahegn Yirgu

Abstract Significant volumes of magma can be intruded into the crust during continental break-up, influencing rift evolution by altering the thermo-mechanical structure of the crust and its response to extensional stresses. Rift magmas additionally feed surface volcanic activity and can be globally significant sources of tectonic CO₂ emissions. Understanding how magmatism may affect rift development requires knowledge on magma intrusion depths in the crust. Here, using data from olivine-hosted melt inclusions, we investigate magma dynamics for basaltic intrusions in the Main Ethiopian Rift (MER). We find evidence for a spatially focused zone of magma intrusion at the MER upper-lower crustal boundary (10–15 km depth), consistent with geophysical datasets. We propose that ascending melts in the MER are intruded over this depth range as discrete sills, likely creating a mechanically weak mid-crustal layer. Our results have important implications for how magma addition can influence crustal rheology in a maturing continental rift.

Plain Language Summary Continental rifting, the break-up of continents to form new ocean basins, is a key component in the tectonic cycle that affects Earth's surface environment. The rifting process is aided by magmatic activity in its final stages, which weakens the crust by heating it. This is believed to facilitate present-day rifting in Ethiopia, where we find rift-related volcanoes. The depth of magma storage in the rifting crust will determine how heat is distributed, and therefore how the physical properties of the crust are altered. Here we study melt inclusions, small pockets of magmas trapped within growing crystals beneath rift volcanoes. Using the concentrations of CO₂ and H₂O in melt inclusions we infer the pressures (and therefore depths) that they formed. Our results demonstrate that magmas rising through the Ethiopian crust consistently stall at a depth range of 10–15 km beneath the surface. Furthermore, the diverse chemical composition of our melt inclusions show that magmas are stored in multiple small bodies versus a larger mixed magma reservoir. This study therefore provides new insights into how magmas are stored in the Ethiopian crust before volcanic eruptions and suggests that rising magmas may produce a weak layer in the middle of the rifting crust.

1. Introduction

Continental rifting involves the rupture of strong continental lithosphere to form new ocean basins. Evidence from active continental rifts and passive margins suggests that continental break-up often involves intrusion of substantial volumes of magma into the rifting crust (e.g., Bastow et al., 2011; Bastow & Keir, 2011; White et al., 2008). These magmas can accommodate extension via dyke intrusion and, depending on their distribution in space and time, may alter the thermo-mechanical structure of the crust (e.g., Buck, 2006; Daniels et al., 2014; Lavecchia et al., 2016; Muluneh et al., 2020). Determining how intruded melts accumulate during rift development is therefore crucial for understanding how the rheology and density structure of the crust evolves with progressive rifting, which in turn has a strong influence on how the crust responds to far-field extensional stresses during non-magmatic and magmatic rifting regimes (e.g., Bialas et al., 2010; Oliveira et al., 2022; Tetreault & Buiter, 2018).

Although the syn-rift interplay between magmatism and tectonics is a key ingredient in facilitating continental break-up (e.g., Bastow & Keir, 2011; Thybo & Nielsen, 2009), observational constraints on basaltic intrusion

© 2023. The Authors.

This is an open access article under the terms of the [Creative Commons Attribution License](https://creativecommons.org/licenses/by/4.0/), which permits use, distribution and reproduction in any medium, provided the original work is properly cited.

Supervision: David Ferguson, Daniel Morgan, Marie Edmonds, Gezahegn Yirgu

Visualization: Kevin Wong, Penny Wieser

Writing – original draft: Kevin Wong, David Ferguson

Writing – review & editing: Kevin Wong, David Ferguson, Daniel Morgan, Marie Edmonds, Amdemichael Zafu Tadesse, Gezahegn Yirgu, Jason Harvey, Samantha Hammond

depths in active rifts obtained through petrology and geochemistry remain limited. While geophysical observations can infer depths of intrusion and crustal melt storage (e.g., through seismicity concurrently triggered during emplacement; Keir et al., 2006; Ebinger et al., 2008), only petrological observations, obtained from basaltic materials derived directly from the intruding melts themselves, can provide first-hand evidence of the magmatic conditions associated with crustal emplacement.

The Main Ethiopian Rift (MER), comprising the northernmost sector of the East African Rift system (EARS), provides a natural laboratory to examine the interplay between rift geodynamics and magmatic intrusion. This late-stage continental rift, which bridges the large fault-bound grabens of the Kenyan Rift and inferred incipient seafloor spreading in Afar (Figure 1a), has been extensively studied through multiple geophysical approaches (e.g., Bastow et al., 2011; Lavayssière et al., 2018; Wright et al., 2016). These studies suggest that significant magma intrusion has occurred in the MER lithosphere, focused under ~20 km-wide and ~60 km-long magmatic-tectonic segments (e.g., Bastow et al., 2011), where as much as half of the crustal volume may comprise new igneous material (Daniels et al., 2014; Maguire et al., 2006). The compositional and thermal effects of magma intrusion may modify the response of the Ethiopian crust to extension, controlling where and how strain is localized as rifting proceeds (e.g., Bastow & Keir, 2011; Lavecchia et al., 2016). Furthermore, degassing of intruded melts during and after emplacement contributes to the significant diffuse CO₂ fluxes measured in the MER (Hunt et al., 2017).

In this study we use petrological methods to investigate the storage depths and compositional diversity of intruded basaltic magmas in the northern MER. Our constraints on magma intrusion conditions are derived from analysis of olivine-hosted silicate melt inclusions (MIs), which are small pockets of quenched magma trapped within growing crystals during crustal magma storage (e.g., Wallace et al., 2021). Unlike erupted lavas, MIs can preserve magmatic volatile contents (e.g., CO₂, H₂O etc., Wallace et al., 2021), allowing volatile saturation pressures, and therefore magmatic storage depths, to be determined (e.g., Ghiorsio & Gualda, 2015). Of particular importance is the volatile species CO₂, which degases strongly with decreasing pressure in basaltic magmas (e.g., Dixon et al., 1995). Continental rifts, including the MER, are known to be significant sources of passively degassing magmatic CO₂ (Foley & Fischer, 2017; Hunt et al., 2017; Lee et al., 2016). By considering the total CO₂ in MIs, entrapped within both glass and bubble, we provide new well-constrained petrological estimates of basaltic intrusion pressures in the MER.

2. Materials and Methods

Our samples are scoriae from the Quaternary basaltic cone field located in the Gedemsa magmatic segment of the MER adjacent to the Boku Volcanic Complex (Figure 1; Tadesse et al., 2019; Nigussie, Alemu, et al., 2023). Littering the remnants of the collapsed ~500 ka Boku caldera, the later-stage ~200 ka basaltic cones and fissure flows are associated with seismic anomalies (e.g., Keranen et al., 2004), gravity anomalies (e.g., Nigussie et al., 2022; Nigussie, Mickus, et al., 2023), and rift-aligned faults characteristic of MER magmatic segments (e.g., Rooney et al., 2011). Quarries provide access into the interiors of cones, where fresh glassy basaltic scoria can be sampled.

Olivine crystals from two cones (Figure 1) were picked from disaggregated scoria, individually polished to 0.25 μm grade on glass slides to expose MIs, and mounted in epoxy resin. We have measured the compositions of 40 MIs (full methods in Supporting Information S1). 27 of these MIs contain CO₂-rich vapor bubbles, which form from post-entrapment changes in pressure, volume and temperature (e.g., MacLennan, 2017; Moore et al., 2015). Bubbles can host a significant fraction of the MI CO₂ budget (e.g., Hartley et al., 2014; Wieser et al., 2021). To estimate the total CO₂ in MIs, essential for accurate barometry, 18 MIs were additionally assessed for bubble CO₂ density using Raman spectroscopy. Our approach differs from previous studies considering MIs from the EARS in this regard, which have opted to either (a) experimentally rehomogenize the bubble (Head et al., 2011; Hudgins et al., 2015), (b) use CO₂ equation of state methods (Rooney et al., 2022), or (c) select MIs without vapor bubbles wherever possible (Field, Barnie, et al., 2012; Field, Blundy, et al., 2012; A. Donovan et al., 2017; Iddon & Edmonds, 2020). Benefiting from recent developments in the calibration of the Raman method through the use of standard materials (e.g., Lamadrid et al., 2017; Wieser et al., 2021), the primary advantage of our approach is the direct measurement of bubble CO₂ without making assumptions concerning post-entrapment processes or experimentally modifying MI glass compositions, which will introduce uncertainties that are difficult to assess and quantify (Rasmussen et al., 2020; Wieser et al., 2021). In addition, by selecting bubble-hosting MIs we avoid

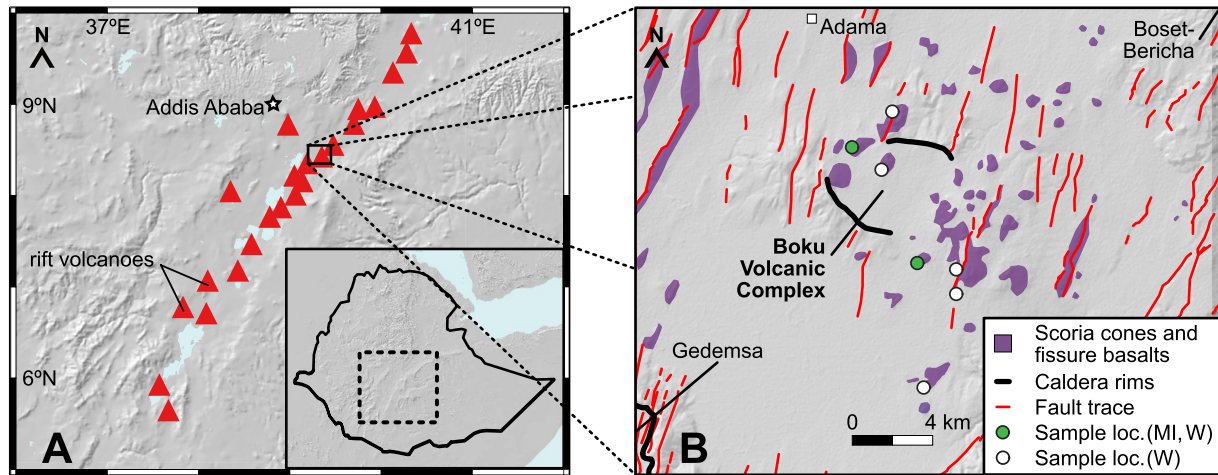


Figure 1. (a) Overview map of the MER, highlighting the location of the Boku Volcanic Complex. Inset figure shows area presented in subfigure (a) within Ethiopia. (b) Simplified geological map of Boku within the Gedemsa magmatic segment, with melt inclusion (MI) and whole-rock (W) sample localities shown. Digital elevation models are GTOPO30 (a; Gesch et al., 1999) and SRTM (b; Farr et al., 2007). Volcano locations in subfigure (a) are obtained from the Global Volcanism Program, Smithsonian Institution (<https://volcano.si.edu/>). Faults in subfigure b of Agostini et al. (2011).

biases towards magmatic conditions that favor bubble-free MIs, which may not be representative of crustal melt storage. By doing so, we provide robust estimates of total CO_2 in MIs, which can be used to determine crustal melt storage pressures.

After Raman spectroscopy, all MIs were analyzed for trace and volatile elements in the glass phase by secondary ion mass spectrometry, followed by electron probe microanalysis to assess major element compositions of MI glass, carrier melt, and host olivine crystals. MI compositions were corrected for post-entrapment crystallization (PEC) using Petrolog3 software (Danyushevsky & Plechov, 2011, see Supporting Information S1). The total CO_2 of MIs is calculated by mass balance using the CO_2 measured in the MI bubble and glass (e.g., Hartley et al., 2014). To complement the MI compositional data set, we have additionally assessed major and trace element whole-rock compositions of basalts collected from several scoria cones and fissure flows in the region using x-ray fluorescence and solution inductively coupled plasma mass spectrometry respectively. All standards and geochemical data are presented in Data Set S1.

3. Results

3.1. Magma Intrusion Depths in the Main Ethiopian Rift

Our key barometric and geochemical results are presented in Figures 2 and 3 (additional figures in Supporting Information S1). MIs are entrapped within olivine crystals of composition Fo_{76-88} , and there are no systematic differences in major, trace, or volatile element concentrations between MIs collected from the two cones in this study (Data Set S1). CO_2 concentrations range from 35 to 5,770 ppm in MI glass only; MIs with CO_2 measurements in both the glass and vapor bubble have total combined CO_2 contents of 1,895–3,248 ppm, with 15%–46% of the CO_2 residing within the bubble (Data Set S1). Where an unanalyzed shrinkage bubble is present, CO_2 contents are assumed to be minima and we estimate the plausible range of total CO_2 using our bubble CO_2 density measurements (see Supporting Information S1). H_2O concentrations display less variability: discounting the three MIs that have clearly degassed (containing ≤ 0.4 wt% H_2O), MIs have mean H_2O of 1.1 ± 0.2 wt% (Figure S6 in Supporting Information S1), which is comparable to H_2O concentrations obtained from other MER and EARS MIs (Iddon & Edmonds, 2020; Rooney et al., 2022).

Volatile saturation pressures of MIs are calculated using the fully thermodynamic MagmaSat volatile solubility model (Ghiorso & Gualda, 2015) via the Python library VESICAL (Iacovino et al., 2021; Wieser et al., 2022). Other volatile solubility models are considered in Supporting Information S1. Entrapment pressures for MIs for which total CO_2 contents are known (vapor bubble and glass), determined at a magmatic temperature of $1,200^\circ\text{C}$ (Iddon et al., 2019; Wong et al., 2022), vary over a relatively narrow range from 2.5 to 4.5 kbar (Figure 2a). In

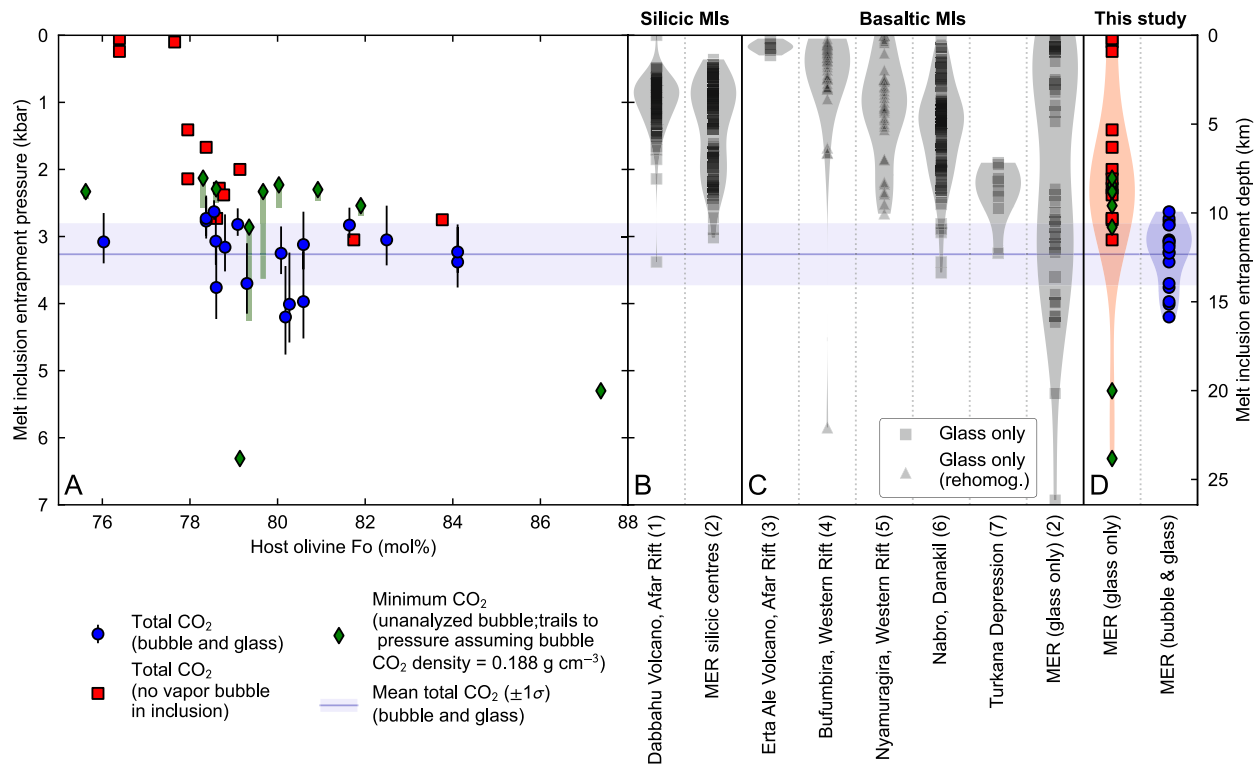


Figure 2. (a) Volatile CO₂-H₂O saturation pressures of olivine-hosted MIs from the MER plotted against MI olivine host composition (olivine Fo = 100-Mg/[Fe + Mg]). MIs are categorized by analyzed components. MIs analyzed for glass CO₂ but not bubble CO₂ (green diamonds) show trails to pressures assuming the mean bubble CO₂ density of our sample set (0.188 g cm⁻³; see Supporting Information S1). Error bars on pressures calculated from MIs for which bubble and glass are analyzed are 1σ. (b–d) Violin plots of volatile CO₂-H₂O saturation pressures recorded by mineral-hosted MIs from the EARS and Afar calculated using MagmaSat (Ghiorso & Gualda, 2015). Saturation pressures are individually determined for each MI using their recorded major and trace element composition and magmatic temperatures. Where FeO_v is provided without Fe₂O₃ all Fe is assumed to be Fe²⁺. Subfigure B shows distributions of silicic MIs (SiO₂ > 60 wt%), subfigure C shows basaltic MIs (SiO₂ < 55 wt%), and subfigure D shows the basaltic MIs of this study. Subfigures B and C consider CO₂ and H₂O in melt inclusion glass only, including experimentally rehomogenized inclusions (triangle markers). The blue line and shaded area across all subfigures marks the mean and 1σ of the MI subset of this study with combined vapor bubble and glass CO₂. References: 1. Field, Blundy, et al. (2012); 2. Iddon and Edmonds (2020); 3. Field, Barrie, et al. (2012); 4. Hudgins et al. (2015); 5. Head et al. (2011); 6. (a) Donovan et al. (2017); 7. Rooney et al. (2022), without bubble corrections.

the MER these pressures correspond to depths of ~10–15 km (assuming a constant upper-mid crustal density of 2.79 g cm⁻³; Cornwell et al., 2006), among the deepest recorded volatile saturation depths for continental rift magmas (Figures 2b–2d). Pressures recorded by MIs without bubbles overlap partially with those that do have analyzed bubbles; however, the average CO₂ concentration and therefore pressure of MIs without a bubble is typically lower than those with a bubble. Two MIs for which only inclusion glass CO₂ is known record higher pressures in excess of 5 kbar (~20 km), corresponding to the MER lower crust. Overall, our barometric results show a relatively limited distribution of magma storage depths with a narrowly focused zone of intrusion centered at ~12 km depth, coincident with the seismically imaged boundary between the upper and lower crust in the MER (Maguire et al., 2006), and in close agreement with MI volatile saturation pressures from the Turkana Depression south of the MER (Figure 2c; Rooney et al., 2022).

3.2. Melt Inclusion Trace Element Compositions

The major element compositions of MIs overlap with carrier basalt compositions and whole-rock compositions of erupted lavas (Data Set S1; Tadesse et al., 2019; Nicotra et al., 2021). Incompatible trace element concentrations vary considerably in both MIs and lavas, but nonetheless still overlap (Figures 3a and 3b). Greater primary compositional variability is preserved in MIs over whole rocks, for example, the ratios La/Yb and Dy/Yb (Figures 3c and 3d), which persists to lower MgO in MIs.

By comparing CO₂ concentrations with trace elements with similar behavior during mantle melting (e.g., Ba, Rb), CO₂ degassing from mantle melts can be assessed (e.g., Le Voyer et al., 2018). While primary magmatic CO₂

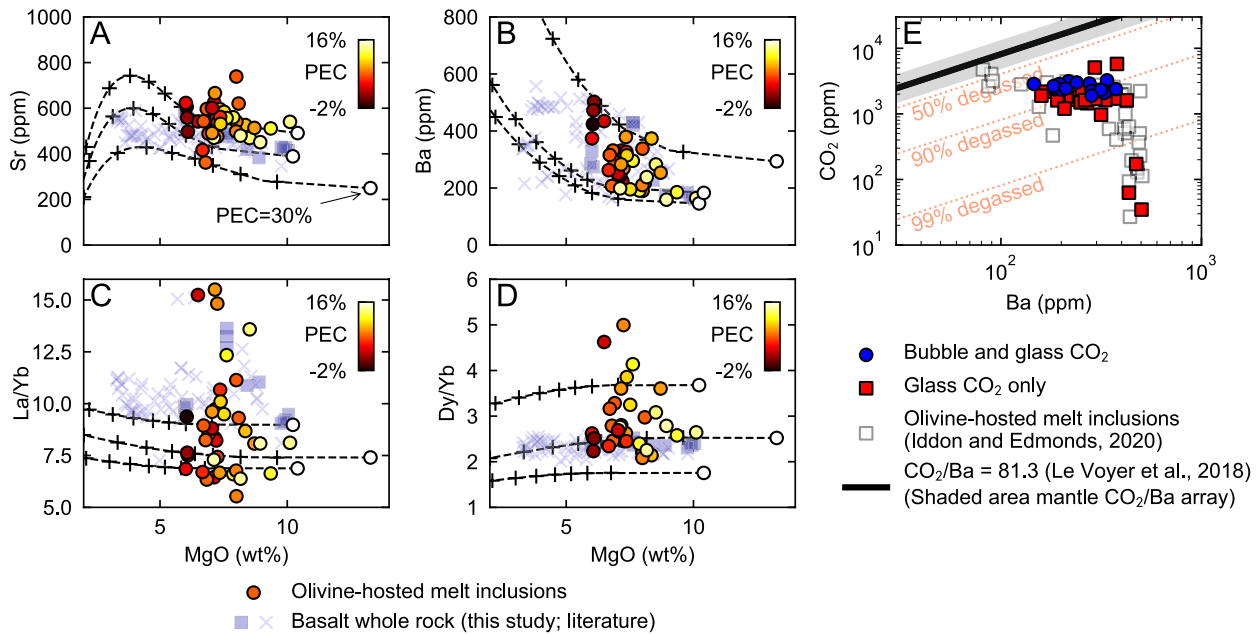


Figure 3. A–D. MI and whole-rock trace element and trace element ratios plotted against MgO (this study; Tadesse et al., 2019; Nicotra et al., 2021). Liquid lines of descent with crosses denoting 10% fractionation intervals are determined from our three highest MgO melts using Rhyolite-MELTS v1.2.0 (Gualda et al., 2012, see Supporting Information S1), assuming Rayleigh fractionation with the partition coefficients collated by Iddon and Edmonds (2020). PEC corrections are detailed in Supporting Information S1. E. Olivine-hosted MI CO₂ plotted against Ba. Degassing lines plotted from primary CO₂/Ba of MORB (81.3; Le Voyer et al., 2018), with shaded area representing range of mantle CO₂/Ba (48.3–133 Rosenthal et al., 2015; Hauri et al., 2017).

contents are not known for MER magmas, the highest observed CO₂/Ba and CO₂/Rb ratios approach the mantle values inferred from undegassed MORB and Icelandic lavas (Rosenthal et al., 2015; Hauri et al., 2017; Le Voyer et al., 2018). Assuming that initial CO₂-trace element ratios are somewhat similar to other mantle-derived melts, CO₂/Ba systematics for MER MIs clearly show evidence for significant degassing of CO₂ prior to entrapment, with ~50%–95% of initial CO₂ likely having been exsolved during ascent to mid-crustal pressures (Figure 3e).

4. Discussion

4.1. Depths of Intrusion in the East African Rift

Our total CO₂ saturation pressures determined from vapor bubble and glass are in broad agreement with maximum pressures of melt storage estimated from MI volatiles at other EARS sectors (see Figures 2b–2d). Applying the same volatile solubility modelling performed on our MIs to literature datasets, we determine that our proposed 10–15 km depth range for basalt storage coincides with the deepest MIs at other parts of the EARS and Afar Rift (Figure 2c; e.g., A. Donovan et al., 2017; Rooney et al., 2022). Geophysical observations of crustal melt movement suggests that melt focusing at these pressures may be ubiquitous within the Eastern Branch of the EARS in addition to the MER (Reiss et al., 2021, 2022; Weinstein et al., 2017).

The lack of evidence for significant melt storage within the upper crust in our data set contrasts with the depth distributions for magma storage obtained from suites of MIs collected at large caldera-forming volcanic centers found along the MER (Figure 2; Iddon & Edmonds, 2020). Under these silicic centers, melt storage appears to extend upwards into the upper crust, where evolved magmas are generated via low pressure fractionation (Iddon & Edmonds, 2020). Notably, the maximum storage depths under caldera complexes in the EARS identified both from MI volatile saturation barometry (Figure 2; Iddon & Edmonds, 2020; Rooney et al., 2022) and from mineral barometry (Iddon et al., 2019; Rooney et al., 2005) coincides with the 10–15 km depth range observed in our data set. This depth range may therefore be the locus of initial basaltic melt emplacement along the MER, with important implications for heat distribution within the rifting crust and therefore crustal strength profiles (Buck, 2006; Daniels et al., 2014; Lavecchia et al., 2016), such as the creation of a mid-crustal weak layer (Muluneh et al., 2020). With the exception of those below caldera complexes/silicic volcanoes (e.g., Biggs

et al., 2011), upper crustal melt bodies (<10 km depth) in the MER are likely to be ephemeral, perhaps forming during periodic intrusive-eruptive episodes (e.g., Ebinger et al., 2013).

In contrast to the extensive MI data corresponding to mid-crustal pressures, very few MIs from our data set and the MER data set of Iddon and Edmonds (2020) record pressures corresponding to the lower crust or Moho (Figure 2; e.g., Maguire et al., 2006; Lavayssière et al., 2018). Considering the evolved compositions of our olivines (mean Fo_{80}) relative to Fo_{90} olivines in other MER volcanic materials (e.g., Rooney et al., 2005), we posit that an initial stage of fractionation near the Moho prior to ascent to mid-crustal pressures is necessary. This hypothesis is supported by low wavespeeds observed at Moho depths from the presence of melt in the heavily intruded lower crust (Chambers et al., 2019; Keranen et al., 2009), and numerical models suggesting that the lowermost crust is weak, hot and underlies a lower-crustal brittle-ductile transition at 20–25 km (Lavecchia et al., 2016; Muluneh et al., 2020). Melts pooling and fractionating at the base of the crust may bypass the ductile lowermost crust entirely if both density differences between melt and crust and lower crustal strain rates are sufficiently high (Muluneh et al., 2021).

Deep CO_2 degassing in the MER, likely derived from degassing of magmas as they ascend towards the weak mid-crust, is focused along discrete fault zones (Hunt et al., 2017; Raggiunti et al., 2023). By making assumptions on the volumes of melt intruded into the crust (e.g., Iddon & Edmonds, 2020), we determine that the difference between expected CO_2 concentrations in primary mantle melts and those recorded in MIs is sufficient to generate the CO_2 fluxes measured from surface degassing (Figure 3e Hunt et al., 2017, see Supporting Information S1). The restriction of significant degassing to localized regions in the MER (Hunt et al., 2017) may suggest that some regions are subject to active intrusion at the present day whereas other portions are not. Future studies should aim to constrain this periodicity of melt emplacement.

4.2. Compositional Heterogeneity in Melt Inclusions

Variability in absolute trace element concentrations (Figures 3a and 3b) could result from fractional crystallization of distinct parental melts and/or mixing between variably fractionated melts with distinct origins. In contrast, the broader distribution of trace element ratios observed in MIs relative to whole rocks (Figures 3c and 3d) can only be inherited from the compositional heterogeneity of parental mantle-derived melts. Such variability, derived from the melting of multiple source lithologies (e.g., Shorttle & MacLennan, 2011) and/or unmixed fractional mantle melts (e.g., Gurenko & Chaussidon, 1995), is preserved at lower MgO contents.

Physical interactions between intrusive bodies therefore appear to be restricted, and we infer that intruded magmas reside in a series of discrete bodies emplaced over a relatively narrow depth range. The slightly lower degree of compositional diversity observed in erupted lavas (Figures 3c and 3d), even at higher MgO, suggests that some mixing does occur prior to eruption and that dyke intrusion into the upper crust may involve partially homogenized melts sourced from multiple mid-crustal sills. Erupted melts extend to lower MgO than the MIs (after PEC corrections), and pre-eruptive mixing and homogenization therefore likely occurs during a final stage of differentiation within upper crustal magma bodies.

4.3. Basaltic Melt Focusing in the Main Ethiopian Rift

The barometric and compositional data from our MIs suggest that intrusion in the MER crust is characterized by emplacement of multiple discrete magma bodies over a relatively narrow depth range coincident with the seismically identified upper-lower crustal boundary. Although our results do not directly constrain the geometry of intrusive bodies, we suggest, based on the narrow range of MI entrapment depths, that these are likely mid-crustal sill complexes. This model is supported by geophysical observations of the MER crust. Strong horizontally oriented seismic anisotropy observed in the MER at depths of 5–15 km is consistent with the presence of sills (Bastow et al., 2010; Chambers et al., 2021; Kendall et al., 2006). Low seismic moment earthquakes in northern MER magmatic segments are distributed within a narrow depth band between 8 and 16 km and have been interpreted as being triggered by movement or emplacement of mid-crustal melts (Daly et al., 2008; Keir et al., 2006). High- V_p , high- V_p/V_s and high-density bodies are inferred to be present at these depths under Boku and other MER segments (Cornwell et al., 2006; Daly et al., 2008; Keranen et al., 2004; Nigussie et al., 2022), as are high-conductivity crustal anomalies (Whaler & Hautot, 2006), all indicative of partially molten mid-crustal intrusions. Our results are also in good agreement with empirical observations relating MER cone clustering to

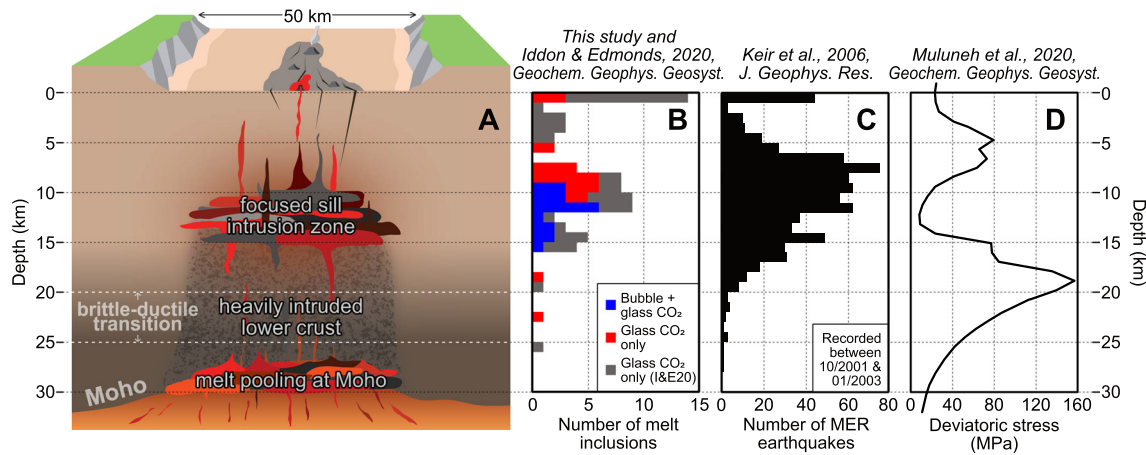


Figure 4. (a) Summary cartoon illustrating our proposed structure of the MER crust. Horizontal and vertical dimensions not to same scale. (b) Histogram of MER olivine-hosted MI saturation pressures (this study; Iddon & Edmonds, 2020). (c) Histogram of MER earthquakes recorded between October 2001 and January 2003 (Keir et al., 2006; Daly et al., 2008, selection criteria in Figure S9 in Supporting Information S1). (d) Numerical model of MER crustal deviatoric stress (Muluneh et al., 2020).

intrusion depths (Mazzarini et al., 2013). To summarize, the melt storage depths resolved directly using petrological methods concur closely with the deepest intrusion pressures determined using geophysical techniques.

Focusing of ascending basaltic melts at this depth range can, to a first order, be attributed to MER crustal density structure, as the mean density of the lower crust exceeds that of our MIs (mean of 2.708 g cm^{-3} , calculated after PEC corrections using DensityX, Iacovino and Till (2019); cf. e.g., Cornwell et al. (2006)). Driven by density differences, basaltic melts will rise to mid-crustal depths before they achieve neutral buoyancy, stall and crystallize. The upper crust, comparatively less dense than the lower crust, will limit the ascent of basalt melts beyond the focusing zone (Cornwell et al., 2006; Mickus et al., 2007).

Melt focusing in the mid-crust could also be attributed to the rheological structure of the crust. Numerical models based on seismic observations suggest that the 10–15 km depth range resolved using our MIs coincides with the weakest part of the Ethiopian crust, which is sandwiched between two strong brittle layers in the upper and mid-lower crust (Muluneh et al., 2020). The strong, lower-density brittle crust above this ductile zone, combined with the density limitations discussed above, likely inhibits further ascent of the buoyant melt (Cornwell et al., 2006; Muluneh et al., 2020). Melt may only progress directly to the surface through the breaking of dyke-induced faults (e.g., Casey et al., 2006), by exploiting pre-existing crustal weaknesses (e.g., Le Corvec et al., 2013), or after extensive fractionation to form lower-density silicic melts (e.g., Gleeson et al., 2017).

We therefore hypothesize that the intrusion and emplacement of melts into this weak, ductile mid-crust will have a strong effect on the overall rheology of the rifting crust, which in turn may govern how the crust locally accommodates strain in response to far-field extensional stresses. Ductile stretching may accommodate crustal deformation at a different rate or manner relative to the brittle layers above and below this weak zone, in turn possibly dictating that future batches of melt are focused in the same region. Indeed, the development of crustal sill systems in the MER may arise from pulsed emplacement of magmas from the lower crust or mantle (e.g., Annen et al., 2015). Stacked sills formed in this manner may maintain high localized temperatures in the crust, which can facilitate further intrusion of melt at shallower pressures, or may themselves contract during cooling to generate accommodation space for further intrusions (Magee et al., 2016). Future numerical or analog models of rift deformation in Ethiopia must account for the development of a hot, ductile, weak layer in the crust, and the influences such a layer may have on overall crustal rheology.

5. Summary

The results of our study are summarized in Figure 4. Through the careful analysis of major, trace, and volatile elements in olivine-hosted MIs, we propose that stacked mid-crustal sills in the depth range of 10–15 km are the dominant form of magmatic storage in the MER (Figures 4a and 4b). Intrusions are known to be discrete

and horizontally oriented from trace element variability (Figure 3) and seismic anisotropy respectively (e.g., Chambers et al., 2021), and develop as a consequence of repeated magmatic intrusion into the mid-crust during the progression of late-stage continental rifting. Initially crystallizing at or near the Moho, mantle-derived magmas bypass the ductile lowermost crust to arrive at the Ethiopian mid-crust, heralded by seismic activity during emplacement (Figure 4c). These melts, stored as discrete sills in the weak, ductile mid-crust, are blocked from further ascent by a strong, lower density upper crust (Figure 4d). The diverse range of trace element ratios observed in MIs gives evidence to limited melt mixing in the crust; partial mixing of magmas between sills may occur in the shallow crust prior to eruption (Figure 3). Petrological evidence for mid-crustal sills in the MER presented in this study is in agreement with geophysical observations (e.g., Keranen et al., 2004), and the volatile composition of basalts comprising these bodies are consistent with CO₂ degassing rates measured at the rift floor (Hunt et al., 2017). The presence of hot sills in the MER mid-crust has important implications for how intruding melts in late-stage rifts affect and are affected by the rheological structure of the crust, and should be considered a key element in future development of continental rifting models.

Data Availability Statement

The complete data set of geochemical analyses and melt inclusion microscope photographs is available within a Zenodo repository (<https://doi.org/10.5281/zenodo.7930488>).

Acknowledgments

KW and PW are funded by NERC DTP studentships NE/L002574/1 and NE/L002507/1 respectively. KW acknowledges additional support from the Geologists' Association New Researchers Award. SIMS analyses are funded through NERC grant IMF694/1119 awarded to DF. ME acknowledges the support of COMET via NERC. We thank Cristina Talavera Rodriguez and Lesley Neve for performing geochemical analyses on our behalf during the COVID-19 pandemic. Yared Sinetebeb, Harri Wyn Williams, Emilie Ringe, and Richard Walsh are thanked for assistance with fieldwork, sample preparation, Raman spectroscopy, and EPMA respectively. We acknowledge thought-provoking discussions with Ian Bastow, Emma Chambers, Tim Craig, Sophie Hautot, Derek Keir, Tyrone Rooney, and Kathy Whaler, and constructive comments from James Muirhead and Ameha Muluneh on an earlier version of this manuscript. Finally, we acknowledge the Ethiopian Ministry of Mines and Oromia State Administration for sampling and field permissions.

References

- Agostini, A., Bonini, M., Corti, G., Sani, F., & Mazzarini, F. (2011). Fault architecture in the Main Ethiopian Rift and comparison with experimental models: Implications for rift evolution and Nubia–Somalia kinematics. *Earth and Planetary Science Letters*, 301(3), 479–492. <https://doi.org/10.1016/j.epsl.2010.11.024>
- Annen, C., Blundy, J. D., Leuthold, J., & Sparks, R. S. J. (2015). Construction and evolution of igneous bodies: Towards an integrated perspective of crustal magmatism. *Lithos*, 230, 206–221. <https://doi.org/10.1016/j.lithos.2015.05.008>
- Bastow, I. D., & Keir, D. (2011). The protracted development of the continent–ocean transition in Afar. *Nature Geoscience*, 4(4), 248–250. <https://doi.org/10.1038/ngeo1095>
- Bastow, I. D., Keir, D., & Daly, E. (2011). The Ethiopia Afar Geoscientific Lithospheric Experiment (EAGLE): Probing the transition from continental rifting to incipient seafloor spreading. In *Geological society of America special papers*. In *Geological Society of America* (Vol. 478, pp. 51–76). [https://doi.org/10.1130/2011.2478\(04\)](https://doi.org/10.1130/2011.2478(04))
- Bastow, I. D., Piliidou, S., Kendall, J.-M., & Stuart, G. W. (2010). Melt-induced seismic anisotropy and magma assisted rifting in Ethiopia: Evidence from surface waves. *Geochemistry, Geophysics, Geosystems*, 11(6), Q0AB05. <https://doi.org/10.1029/2010GC003036>
- Bialas, R. W., Buck, W. R., & Qin, R. (2010). How much magma is required to rift a continent? *Earth and Planetary Science Letters*, 292(1), 68–78. <https://doi.org/10.1016/j.epsl.2010.01.021>
- Biggs, J., Bastow, I. D., Keir, D., & Lewi, E. (2011). Pulses of deformation reveal frequently recurring shallow magmatic activity beneath the Main Ethiopian Rift. *Geochemistry, Geophysics, Geosystems*, 12(9), Q0AB10. <https://doi.org/10.1029/2011GC003662>
- Buck, W. R. (2006). The role of magma in the development of the Afro-Arabian Rift system. In G. Yirgu, C. Ebinger, & P. K. H. Maguire (Eds.), *The Afar volcanic province within the East African Rift system* (Vol. 259, pp. 43–54). Retrieved from <http://sp.lyellcollection.org/content/259/1/43>
- Casey, M., Ebinger, C., Keir, D., Gloaguen, R., & Mohamed, F. (2006). Strain accommodation in transitional rifts: Extension by magma intrusion and faulting in Ethiopian rift magmatic segments. In G. Yirgu, C. J. Ebinger, & P. K. H. Maguire (Eds.), *The Afar volcanic province within the East African Rift system* (Vol. 259, pp. 143–163). Retrieved from <http://sp.lyellcollection.org/content/259/1/143>
- Chambers, E. L., Harmon, N., Keir, D., & Rychert, C. A. (2019). Using ambient noise to image the northern East African Rift. *Geochemistry, Geophysics, Geosystems*, 20(4), 2091–2109. <https://doi.org/10.1029/2018GC008129>
- Chambers, E. L., Harmon, N., Rychert, C. A., & Keir, D. (2021). Variations in melt emplacement beneath the northern East African Rift from radial anisotropy. *Earth and Planetary Science Letters*, 573, 117150. <https://doi.org/10.1016/j.epsl.2021.117150>
- Cornwell, D. G., Mackenzie, G. D., England, R. W., Maguire, P. K. H., Asfaw, L. M., & Oluma, B. (2006). Northern Main Ethiopian Rift crustal structure from new high-precision gravity data. *The Afar Volcanic Province within the East African Rift System*, 259(1), 307–321. <https://doi.org/10.1144/gsl.sp.2006.259.01.23>
- Daly, E., Keir, D., Ebinger, C. J., Stuart, G. W., Bastow, I. D., & Ayele, A. (2008). Crustal tomographic imaging of a transitional continental rift: The Ethiopian rift. *Geophysical Journal International*, 172(3), 1033–1048. <https://doi.org/10.1111/j.1365-246X.2007.03682.x>
- Daniels, K. A., Bastow, I. D., Keir, D., Sparks, R. S. J., & Menand, T. (2014). Thermal models of dyke intrusion during development of continent–ocean transition. *Earth and Planetary Science Letters*, 385, 145–153. <https://doi.org/10.1016/j.epsl.2013.09.018>
- Danyushevsky, L. V., & Plechov, P. (2011). Petrolog3: Integrated software for modeling crystallization processes. *Geochemistry, Geophysics, Geosystems*, 12(7), Q07021. <https://doi.org/10.1029/2011GC003516>
- Dixon, J. E., Stolper, E. M., & Holloway, J. R. (1995). An experimental study of water and carbon dioxide solubilities in mid-ocean ridge basaltic liquids. Part I: Calibration and solubility models. *Journal of Petrology*, 36(6), 1607–1631. <https://doi.org/10.1093/oxfordjournals.petrology.a037267>
- Donovan, A., Blundy, J., Oppenheimer, C., & Buisman, I. (2017). The 2011 eruption of Nabro volcano, Eritrea: Perspectives on magmatic processes from melt inclusions. *Contributions to Mineralogy and Petrology*, 173(1), 1. <https://doi.org/10.1007/s00410-017-1425-2>
- Ebinger, C. J., Keir, D., Ayele, A., Calais, E., Wright, T. J., Belachew, M., et al. (2008). Capturing magma intrusion and faulting processes during continental rupture: Seismicity of the Dabbahu (Afar) rift. *Geophysical Journal International*, 174(3), 1138–1152. <https://doi.org/10.1111/j.1365-246X.2008.03877.x>
- Ebinger, C. J., van Wijk, J., & Keir, D. (2013). The time scales of continental rifting: Implications for global processes. In *Geological society of America special papers*. In *Geological Society of America* (Vol. 500, pp. 371–396). [https://doi.org/10.1130/2013.2500\(11\)](https://doi.org/10.1130/2013.2500(11))

- Farr, T. G., Rosen, P. A., Caro, E., Crippen, R., Duren, R., Hensley, S., et al. (2007). The shuttle radar topography mission. *Reviews of Geophysics*, 45(2), RG2004. <https://doi.org/10.1029/2005RG000183>
- Field, L., Barnie, T., Blundy, J., Brooker, R. A., Keir, D., Lewi, E., & Saunders, K. (2012). Integrated field, satellite and petrological observations of the November 2010 eruption of Erta Ale. *Bulletin of Volcanology*, 74(10), 2251–2271. <https://doi.org/10.1007/s00445-012-0660-7>
- Foley, S. F., & Fischer, T. P. (2017). An essential role for continental rifts and lithosphere in the deep carbon cycle. *Nature Geoscience*, 10(12), 897–902. <https://doi.org/10.1038/s41561-017-0002-7>
- Gesch, D. B., Verdin, K. L., & Greenlee, S. K. (1999). New land surface digital elevation model covers the Earth. *Eos, Transactions American Geophysical Union*, 80(6), 69–70. <https://doi.org/10.1029/99EO00050>
- Ghiorso, M. S., & Gualda, G. A. R. (2015). An H₂O–CO₂ mixed fluid saturation model compatible with rhyolite-MELTS. *Contributions to Mineralogy and Petrology*, 169(6), 53. <https://doi.org/10.1007/s00410-015-1141-8>
- Gleeson, M. L. M., Stock, M. J., Pyle, D. M., Mather, T. A., Hutchison, W., Yirgu, G., & Wade, J. (2017). Constraining magma storage conditions at a restless volcano in the Main Ethiopian Rift using phase equilibria models. *Journal of Volcanology and Geothermal Research*, 337, 44–61. <https://doi.org/10.1016/j.jvolgeores.2017.02.026>
- Gualda, G. A. R., Ghiorso, M. S., Lemons, R. V., & Carley, T. L. (2012). Rhyolite-MELTS: A modified calibration of MELTS optimized for silica-rich, fluid-bearing magmatic systems. *Journal of Petrology*, 53(5), 875–890. <https://doi.org/10.1093/ptrology/egr080>
- Gurenko, A. A., & Chaussidon, M. (1995). Enriched and depleted primitive melts included in olivine from Icelandic tholeiites: Origin by continuous melting of a single mantle column. *Geochimica et Cosmochimica Acta*, 59(14), 2905–2917. [https://doi.org/10.1016/0016-7037\(95\)00184-0](https://doi.org/10.1016/0016-7037(95)00184-0)
- Hartley, M. E., MacLennan, J., Edmonds, M., & Thordarson, T. (2014). Reconstructing the deep CO₂ degassing behaviour of large basaltic fissure eruptions. *Earth and Planetary Science Letters*, 393, 120–131. <https://doi.org/10.1016/j.epsl.2014.02.031>
- Hauri, E. H., MacLennan, J., McKenzie, D., Gronvold, K., Oskarsson, N., & Shimizu, N. (2017). CO₂ content beneath northern Iceland and the variability of mantle carbon. *Geology*, 46(1), 55–58. <https://doi.org/10.1130/G39413.1>
- Head, E. M., Shaw, A. M., Wallace, P. J., Sims, K. W. W., & Carn, S. A. (2011). Insight into volatile behavior at Nyamuragira volcano (D.R. Congo, Africa) through olivine-hosted melt inclusions. *Geochemistry, Geophysics, Geosystems*, 12(10), Q0AB11. <https://doi.org/10.1029/2011GC003699>
- Hudgins, T. R., Mukasa, S. B., Simon, A. C., Moore, G., & Barifajjo, E. (2015). Melt inclusion evidence for CO₂-rich melts beneath the western branch of the East African Rift: Implications for long-term storage of volatiles in the deep lithospheric mantle. *Contributions to Mineralogy and Petrology*, 169(5), 46. <https://doi.org/10.1007/s00410-015-1140-9>
- Hunt, J. A., Zafu, A., Mather, T. A., Pyle, D. M., & Barry, P. H. (2017). Spatially variable CO₂ degassing in the main Ethiopian Rift: Implications for magma storage, volatile transport, and rift-related emissions. *Geochemistry, Geophysics, Geosystems*, 18(10), 3714–3737. <https://doi.org/10.1002/2017GC006975>
- Iacovino, K., Matthews, S., Wieser, P. E., Moore, G. M., & Bégué, F. (2021). VESICAL Part I: An open-source thermodynamic model engine for mixed volatile (H₂O–CO₂) solubility in silicate melts. *Earth and Space Science*, 8(11), e2020EA001584. <https://doi.org/10.1029/2020EA001584>
- Iacovino, K., & Till, C. B. (2019). DensityX: A program for calculating the densities of magmatic liquids up to 1,627°C and 30 kbar. *Volcanica*, 2(1), 1–10. <https://doi.org/10.30909/vol.02.01.0110>
- Iddon, F., & Edmonds, M. (2020). Volatile-rich magmas distributed through the upper crust in the Main Ethiopian Rift. *Geochemistry, Geophysics, Geosystems*, 21(6), e2019GC008904. <https://doi.org/10.1029/2019GC008904>
- Iddon, F., Jackson, C., Hutchison, W., Fontijn, K., Pyle, D. M., Mather, T. A., et al. (2019). Mixing and crystal scavenging in the Main Ethiopian Rift revealed by trace element systematics in feldspars and glasses. *Geochemistry, Geophysics, Geosystems*, 20(1), 230–259. <https://doi.org/10.1029/2018GC007836>
- Keir, D., Ebinger, C. J., Stuart, G. W., Daly, E., & Ayele, A. (2006). Strain accommodation by magmatism and faulting as rifting proceeds to breakup: Seismicity of the northern Ethiopian rift. *Journal of Geophysical Research*, 111(B5), B05314. <https://doi.org/10.1029/2005JB003748>
- Kendall, J.-M., Pilidou, S., Keir, D., Bastow, I., Stuart, G., & Ayele, A. (2006). Mantle upwellings, melt migration and the rifting of Africa: Insights from seismic anisotropy. In G. Yirgu, C. J. Ebinger, & P. K. H. Maguire (Eds.), *The Afar volcanic province within the East African Rift system* (Vol. 259, pp. 55–72). <https://doi.org/10.1144/GSL.SP.2006.259.01.06>
- Keranen, K. M., Klemperer, S. L., & Gloaguen, R., & EAGLE Working Group. (2004). Three-dimensional seismic imaging of a protoridge axis in the Main Ethiopian rift. *Geology*, 32(11), 949. <https://doi.org/10.1130/G20737.1>
- Keranen, K. M., Klemperer, S. L., Julia, J., Lawrence, J. F., & Nyblade, A. A. (2009). Low lower crustal velocity across Ethiopia: Is the Main Ethiopian Rift a narrow rift in a hot craton? *Geochemistry, Geophysics, Geosystems*, 10(5), Q0AB01. <https://doi.org/10.1029/2008GC002293>
- Lamadrid, H., Moore, L., Moncada, D., Rimstidt, J., Burruss, R., & Bodnar, R. (2017). Reassessment of the Raman CO₂ densimeter. *Chemical Geology*, 450, 210–222. <https://doi.org/10.1016/j.chemgeo.2016.12.034>
- Lavayssière, A., Rychert, C., Harmon, N., Keir, D., Hammond, J. O. S., Kendall, J.-M., et al. (2018). Imaging lithospheric discontinuities beneath the Northern East African Rift using S-to-P receiver functions. *Geochemistry, Geophysics, Geosystems*, 19(10), 4048–4062. <https://doi.org/10.1029/2018GC007463>
- Lavecchia, A., Beekman, F., Clark, S. R., & Cloetingh, S. A. P. L. (2016). Thermo-rheological aspects of crustal evolution during continental breakup and melt intrusion: The Main Ethiopian Rift, East Africa. *Tectonophysics*, 686, 51–62. <https://doi.org/10.1016/j.tecto.2016.07.018>
- Le Corvec, N., Menand, T., & Lindsay, J. (2013). Interaction of ascending magma with pre-existing crustal fractures in monogenetic basaltic volcanism: An experimental approach. *Journal of Geophysical Research: Solid Earth*, 118(3), 968–984. <https://doi.org/10.1002/jgrb.50142>
- Lee, H., Muirhead, J. D., Fischer, T. P., Ebinger, C. J., Kattenhorn, S. A., Sharp, Z. D., & Kianji, G. (2016). Massive and prolonged deep carbon emissions associated with continental rifting. *Nature Geoscience*, 9(2), 145–149. <https://doi.org/10.1038/ngeo2622>
- Le Voyer, M., Hauri, E. H., Cottrell, E., Kelley, K. A., Salters, V. J. M., Langmuir, C. H., et al. (2018). Carbon fluxes and primary magma CO₂ contents along the global mid-ocean ridge system. *Geochemistry, Geophysics, Geosystems*, 20(3), 1387–1424. <https://doi.org/10.1029/2018GC007630>
- MacLennan, J. (2017). Bubble formation and decrepitation control the CO₂ content of olivine-hosted melt inclusions. *Geochemistry, Geophysics, Geosystems*, 18(2), 597–616. <https://doi.org/10.1002/2016GC006633>
- Magee, C., Muirhead, J. D., Karvelas, A., Holford, S. P., Jackson, C. A., Bastow, I. D., et al. (2016). Lateral magma flow in mafic sill complexes. *Geosphere*, 12(3), 809–841. <https://doi.org/10.1130/GES01256.1>
- Maguire, P., Keller, G., Klemperer, S., Mackenzie, G., Keranen, K., Harder, S., et al. (2006). Crustal structure of the northern Main Ethiopian Rift from the EAGLE controlled-source survey; a snapshot of incipient lithospheric break-up. *The Afar Volcanic Province within the East African Rift System*, 259(1), 269–292. <https://doi.org/10.1144/GSL.SP.2006.259.01.21>
- Mazzarini, F., Rooney, T. O., & Isola, I. (2013). The intimate relationship between strain and magmatism: A numerical treatment of clustered monogenetic fields in the main Ethiopian Rift. *Tectonics*, 32(1), 49–64. <https://doi.org/10.1029/2012TC003146>
- Mickus, K., Tadesse, K., Keller, G. R., & Oluma, B. (2007). Gravity analysis of the main Ethiopian rift. *Journal of African Earth Sciences*, 48(2), 59–69. <https://doi.org/10.1016/j.jafrearsci.2007.02.008>

- Moore, L. R., Gazel, E., Tuohy, R., Lloyd, A. S., Esposito, R., Steele-MacInnis, M., et al. (2015). Bubbles matter: An assessment of the contribution of vapor bubbles to melt inclusion volatile budgets. *American Mineralogist*, *100*(4), 806–823. <https://doi.org/10.2138/am-2015-5036>
- Mulneh, A. A., Brune, S., Illsley-Kemp, F., Corti, G., Keir, D., Glerum, A., et al. (2020). Mechanism for deep crustal seismicity: Insight from modeling of deformation processes at the Main Ethiopian Rift. *Geochemistry, Geophysics, Geosystems*, *21*(7), e2020GC008935. <https://doi.org/10.1029/2020GC008935>
- Mulneh, A. A., Keir, D., & Corti, G. (2021). Thermo-rheological properties of the Ethiopian lithosphere and evidence for transient fluid induced lower crustal seismicity beneath the Ethiopian Rift. *Frontiers in Earth Science*, *9*. <https://doi.org/10.3389/feart.2021.610165>
- Nicotra, E., Viccaro, M., Donato, P., Acocella, V., & De Rosa, R. (2021). Catching the Main Ethiopian Rift evolving towards plate divergence. *Scientific Reports*, *11*(1), 21821. <https://doi.org/10.1038/s41598-021-01259-6>
- Nigusie, W., Alemu, A., Mickus, K., & Mulneh, A. A. (2022). Structure of the upper crust at the axis segmentation stage of rift evolution as revealed by gravity data: Case study of the Gedemsa magmatic segment, Main Ethiopian Rift. *Journal of African Earth Sciences*, *190*, 104523. <https://doi.org/10.1016/j.jafrearsci.2022.104523>
- Nigusie, W., Alemu, A., Mulneh, A. A., Mickus, K., Muhabaw, Y., & Ballay, M. (2023). Formation of magmatic segments within the Aluto-Gedemsa area, main Ethiopian Rift. *Italian Journal of Geosciences*, *142*(1), 28–41. <https://doi.org/10.3301/IJG.2023.02>
- Oliveira, M. E., Gomes, A. S., Rosas, F. M., Duarte, J. C., França, G. S., Almeida, J. C., & Fuck, R. A. (2022). Impact of crustal rheology and inherited mechanical weaknesses on early continental rifting and initial evolution of double graben structural configurations: Insights from 2D numerical models. *Tectonophysics*, *831*, 229281. <https://doi.org/10.1016/j.tecto.2022.229281>
- Raggiunti, M., Keir, D., Pagli, C., & Lavayssière, A. (2023). Evidence of fluid induced earthquake swarms from high resolution earthquake relocation in the main Ethiopian rift. *Geochemistry, Geophysics, Geosystems*, *24*(4), e2022GC010765. <https://doi.org/10.1029/2022GC010765>
- Rasmussen, D. J., Plank, T. A., Wallace, P. J., Newcombe, M. E., & Lowenstern, J. B. (2020). Vapor-bubble growth in olivine-hosted melt inclusions. *American Mineralogist*, *105*(12), 1898–1919. <https://doi.org/10.2138/am-2020-7377>
- Reiss, M. C., De Siena, L., & Muirhead, J. D. (2022). The interconnected magmatic plumbing system of the Natron Rift. *Geophysical Research Letters*, *49*(15), e2022GL098922. <https://doi.org/10.1029/2022GL098922>
- Reiss, M. C., Muirhead, J. D., Laizer, A., Link, F., Kazimoto, E., Ebinger, C. J., & Rumpker, G. (2021). The impact of complex volcanic plumbing on the nature of seismicity in the developing magmatic natron rift, Tanzania. *Frontiers in Earth Science*, *8*. <https://doi.org/10.3389/feart.2020.609805>
- Rooney, T. O., Bastow, I. D., & Keir, D. (2011). Insights into extensional processes during magma assisted rifting: Evidence from aligned scoria cones. *Journal of Volcanology and Geothermal Research*, *201*(1), 83–96. <https://doi.org/10.1016/j.jvolgeores.2010.07.019>
- Rooney, T. O., Furman, T., Yirgu, G., & Ayalew, D. (2005). Structure of the Ethiopian lithosphere: Xenolith evidence in the main Ethiopian Rift. *Geochimica et Cosmochimica Acta*, *69*(15), 3889–3910. <https://doi.org/10.1016/j.gca.2005.03.043>
- Rooney, T. O., Wallace, P. J., Muirhead, J. D., Chiasera, B., Steiner, R. A., Girard, G., & Karson, J. A. (2022). Transition to magma-driven rifting in the south Turkana basin, Kenya: Part 2. *Journal of the Geological Society*, *179*(6), jgs2021–160. <https://doi.org/10.1144/jgs2021-160>
- Rosenthal, A., Hauri, E. H., & Hirschmann, M. M. (2015). Experimental determination of C, F, and H partitioning between mantle minerals and carbonated basalt, CO₂/Ba and CO₂/Nb systematics of partial melting, and the CO₂ contents of basaltic source regions. *Earth and Planetary Science Letters*, *412*, 77–87. <https://doi.org/10.1016/j.epsl.2014.11.044>
- Shorttle, O., & MacLennan, J. (2011). Compositional trends of Icelandic basalts: Implications for short-length scale lithological heterogeneity in mantle plumes. *Geochemistry, Geophysics, Geosystems*, *12*(11), Q11008. <https://doi.org/10.1029/2011GC003748>
- Tadesse, A. Z., Ayalew, D., Pik, R., Yirgu, G., & Fontijn, K. (2019). Magmatic evolution of the Boku volcanic complex, Main Ethiopian Rift. *Journal of African Earth Sciences*, *149*, 109–130. <https://doi.org/10.1016/j.jafrearsci.2018.08.003>
- Tetreault, J. L., & Buiter, S. J. H. (2018). The influence of extension rate and crustal rheology on the evolution of passive margins from rifting to break-up. *Tectonophysics*, *746*, 155–172. <https://doi.org/10.1016/j.tecto.2017.08.029>
- Thybo, H., & Nielsen, C. A. (2009). Magma-compensated crustal thinning in continental rift zones. *Nature*, *457*(7231), 873–876. <https://doi.org/10.1038/nature07688>
- Wallace, P. J., Plank, T., Bodnar, R. J., Gaetani, G. A., & Shea, T. (2021). Olivine-hosted melt inclusions: A microscopic perspective on a complex magmatic world. *Annual Review of Earth and Planetary Sciences*, *49*(1), 465–494. <https://doi.org/10.1146/annurev-earth-082420-060506>
- Weinstein, A., Oliva, S. J., Ebinger, C. J., Roecker, S., Tiberi, C., Aman, M., et al. (2017). Fault-magma interactions during early continental rifting: Seismicity of the Magadi-Natron-Manyara basins, Africa. *Geochemistry, Geophysics, Geosystems*, *18*(10), 3662–3686. <https://doi.org/10.1002/2017GC007027>
- Whaler, K. A., & Hautot, S. (2006). The electrical resistivity structure of the crust beneath the northern Main Ethiopian Rift. In G. Yirgu, C. J. Ebinger, & P. K. H. Maguire (Eds.), *The Afar volcanic province within the East African Rift system* (Vol. 259, pp. 293–305). Retrieved from <http://sp.lyellcollection.org/content/259/1/293>
- White, R. S., Smith, L. K., Roberts, A. W., Christie, P. A. F., & Kuszniir, N. J., & The Rest of the iSIMM Team. (2008). Lower-crustal intrusion on the North Atlantic continental margin. *Nature*, *452*(7186), 460–464. <https://doi.org/10.1038/nature06687>
- Wieser, P. E., Iacovino, K., Matthews, S., Moore, G., & Allison, C. M. (2022). VEScal: 2. A critical approach to volatile solubility modeling using an open-source Python3 engine. *Earth and Space Science*, *9*(2), e2021EA001932. <https://doi.org/10.1029/2021EA001932>
- Wieser, P. E., Lamadrid, H., MacLennan, J., Edmonds, M., Matthews, S., Iacovino, K., et al. (2021). Reconstructing magma storage depths for the 2018 Kilauean eruption from melt inclusion CO₂ contents: The importance of vapor bubbles. *Geochemistry, Geophysics, Geosystems*, *22*(2), e2020GC009364. <https://doi.org/10.1029/2020GC009364>
- Wong, K., Ferguson, D., Matthews, S., Morgan, D., Tadesse, A. Z., Sinetebeb, Y., & Yirgu, G. (2022). Exploring rift geodynamics in Ethiopia through olivine-spinel Al-exchange thermometry and rare-Earth element distributions. *Earth and Planetary Science Letters*, *597*, 117820. <https://doi.org/10.1016/j.epsl.2022.117820>
- Wright, T. J., Ayele, A., Ferguson, D. J., Kidane, T., & Vye-Brown, C. (Eds.). (2016). (Eds.), *Magmatic rifting and active volcanism* (Vol. 420).

References From the Supporting Information

- Allison, C. M., Roggensack, K., & Clarke, A. B. (2019). H₂O–CO₂ solubility in alkali-rich mafic magmas: New experiments at mid-crustal pressures. *Contributions to Mineralogy and Petrology*, *174*(7), 58. <https://doi.org/10.1007/s00410-019-1592-4>
- Armitage, J. J., Ferguson, D. J., Goes, S., Hammond, J. O. S., Calais, E., Rychert, C. A., & Harmon, N. (2015). Upper mantle temperature and the onset of extension and break-up in Afar, Africa. *Earth and Planetary Science Letters*, *418*, 78–90. <https://doi.org/10.1016/j.epsl.2015.02.039>
- Blundy, J. D., & Wood, B. J. (1991). Crystal-chemical controls on the partitioning of Sr and Ba between plagioclase feldspar, silicate melts, and hydrothermal solutions. *Geochimica et Cosmochimica Acta*, *55*(1), 193–209. [https://doi.org/10.1016/0016-7037\(91\)90411-W](https://doi.org/10.1016/0016-7037(91)90411-W)

- Danyushevsky, L. V. (2001). The effect of small amounts of H₂O on crystallisation of mid-ocean ridge and Backarc basin magmas. *Journal of Volcanology and Geothermal Research*, 110(3), 265–280. [https://doi.org/10.1016/S0377-0273\(01\)00213-X](https://doi.org/10.1016/S0377-0273(01)00213-X)
- DeVitre, C. L., Barth, A., Gazel, E., Plank, T. A., & Ramalho, R. (2021). Solving the carbonate problem in melt inclusion bubbles. In *AGU fall meeting abstracts*. Retrieved from <https://agu.confex.com/agu/fm21/meetingapp.cgi/Paper/845682>
- DeVitre, C. L., Dayton, K., Gazel, E., Barth, A., Plank, T. A., Pamukcu, A., et al. (2022). Accounting for multi-phase carbon in melt inclusion bubbles. In *Goldschmidt conference abstracts*. Retrieved from <https://conf.goldschmidt.info/goldschmidt/2022/meetingapp.cgi/Paper/12601>
- Dixon, J. E. (1997). Degassing of alkalic basalts. *American Mineralogist*, 82(3–4), 368–378. <https://doi.org/10.2138/am-1997-3-415>
- Donovan, J. J. (2021). Probe for EPMA v. 13.0.5 user's guide and reference (Xtreme Edition). Retrieved from <https://probesoftware.com/download/PROBEWIN.pdf>
- Field, L., Blundy, J., Brooker, R. A., Wright, T., & Yirgu, G. (2012). Magma storage conditions beneath Dabbahu Volcano (Ethiopia) constrained by petrology, seismicity and satellite geodesy. *Bulletin of Volcanology*, 74(5), 981–1004. <https://doi.org/10.1007/s00445-012-0580-6>
- Hauri, E., Wang, J., Dixon, J. E., King, P. L., Mandeville, C., & Newman, S. (2002). SIMS analysis of volatiles in silicate glasses: 1. Calibration, matrix effects and comparisons with FTIR. *Chemical Geology*, 183(1), 99–114. [https://doi.org/10.1016/S0009-2541\(01\)00375-8](https://doi.org/10.1016/S0009-2541(01)00375-8)
- Iacono-Marziano, G., Morizet, Y., Le Trong, E., & Gaillard, F. (2012). New experimental data and semi-empirical parameterization of H₂O–CO₂ solubility in mafic melts. *Geochimica et Cosmochimica Acta*, 97, 1–23. <https://doi.org/10.1016/j.gca.2012.08.035>
- Jarosewich, E. (2002). Smithsonian microbeam standards. *Journal of Research of the National Institute of Standards and Technology*, 107(6), 681–685. <https://doi.org/10.6028/jres.107.054>
- Jochum, K. P., Stoll, B., Herwig, K., Willbold, M., Hofmann, A. W., Amini, M., et al. (2006). MPI-DING reference glasses for in situ microanalysis: New reference values for element concentrations and isotope ratios. *Geochemistry, Geophysics, Geosystems*, 7(2), Q02008. <https://doi.org/10.1029/2005GC001060>
- Kendall, J.-M., Stuart, G. W., Ebinger, C. J., Bastow, I. D., & Keir, D. (2005). Magma-assisted rifting in Ethiopia. *Nature*, 433(7022), 146–148. <https://doi.org/10.1038/nature03161>
- Moore, L. R., Mironov, N., Portnyagin, M., Gazel, E., & Bodnar, R. J. (2018). Volatile contents of primitive bubble-bearing melt inclusions from Klyuchevskoy volcano, Kamchatka: Comparison of volatile contents determined by mass-balance versus experimental homogenization. *Journal of Volcanology and Geothermal Research*, 358, 124–131. <https://doi.org/10.1016/j.jvolgeores.2018.03.007>
- Neave, D. A., Fabbro, G., Herd, R. A., Petrone, C. M., & Edmonds, M. (2012). Melting, differentiation and degassing at the Pantelleria volcano, Italy. *Journal of Petrology*, 53(3), 637–663. <https://doi.org/10.1093/petrology/egr074>
- Newman, S., & Lowenstern, J. B. (2002). VolatileCalc: A silicate melt–H₂O–CO₂ solution model written in visual basic for excel. *Computers & Geosciences*, 28(5), 597–604. [https://doi.org/10.1016/S0098-3004\(01\)00081-4](https://doi.org/10.1016/S0098-3004(01)00081-4)
- Nigusse, W., Mickus, K., Keir, D., Alemu, A., Muhabaw, Y., Muluneh, A. A., et al. (2023). Subsurface structure of magmatic segments during continental breakup: Perspectives from a gravity data analysis along the Main Ethiopian Rift. *Frontiers in Earth Science*, 10. <https://doi.org/10.3389/feart.2022.1092759>
- Saria, E., Calais, E., Stamps, D. S., Delvaux, D., & Hartnady, C. J. H. (2014). Present-day kinematics of the East African Rift. *Journal of Geophysical Research: Solid Earth*, 119(4), 3584–3600. <https://doi.org/10.1002/2013JB010901>
- Schneider, C. A., Rasband, W. S., & Eliceiri, K. W. (2012). NIH image to ImageJ: 25 years of image analysis. *Nature Methods*, 9(7), 671–675. <https://doi.org/10.1038/nmeth.2089>
- Shishkina, T., Botcharnikov, R., Holtz, F., Almeev, R., & Portnyagin, M. (2010). Solubility of H₂O- and CO₂-bearing fluids in tholeiitic basalts at pressures up to 500MPa. *Chemical Geology*, 277(1–2), 115–125. <https://doi.org/10.1016/j.chemgeo.2010.07.014>
- Tucker, J. M., Hauri, E. H., Pietruszka, A. J., Garcia, M. O., Marske, J. P., & Trusdell, F. A. (2019). A high carbon content of the Hawaiian mantle from olivine-hosted melt inclusions. *Geochimica et Cosmochimica Acta*, 254, 156–172. <https://doi.org/10.1016/j.gca.2019.04.001>